ACS APPLIED MATERIALS & INTERFACES

RESEARCH ARTICLE

www.acsami.org

Diketopyrrolopyrrole-Containing Oligothiophene-Fullerene Triads and Their Use in Organic Solar Cells

Teresa L. Chen,[†] Yue Zhang,[†] Patrizia Smith,[‡] Arnold Tamayo,*[,‡] Yi Liu,[†] and Biwu Ma*[,†]

[†]The Molecular Foundry, Lawrence Berkeley National Laboratory, Berkeley, California 94720, United States

[‡]Chemistry and Geochemistry, Colorado School of Mines, Golden, Colorado 80401, United States

Supporting Information

ABSTRACT: We report the characterization of a series of oligothiophene-diketopyrrolopyrrole-fullerene triads and their use as active materials for solution processed organic solar cells (OSCs). By incorporating the diketopyrrolopyrrole (DPP) core with electron rich oligothiophene units and electron withdrawing fullerene units, multifunctional electronic molecules have been prepared; these molecules show high solubility in common organic solvents, excellent photophysical properties with high extinction coefficients (1×10^4 to 1×10^5 M^{-1} cm^{-1}) and broad absorption spectra coverage (250−800 nm), as well as suitable molecular orbital energy levels (HOMO of approximately −5.1 eV, LUMO of approximately −3.7 eV). Solution-processed thin-film organic field effect transistors (OFETs) from these triads revealed good *n*-type characteristics with electron mobilities up to 1.5×10^{-3} cm^2 V^{-1} s^{-1}. With these multifunctional triads, single-component OSCs have been fabricated, exhibiting power conversion efficiencies (PCEs) of up to 0.5 % under AM 1.5 G simulated 1 sun solar illumination. Blending these molecules with poly(3-hexylthiophene) (P3HT) afforded bulk heterojunction OSCs with PCEs reaching as high as 2.41%.

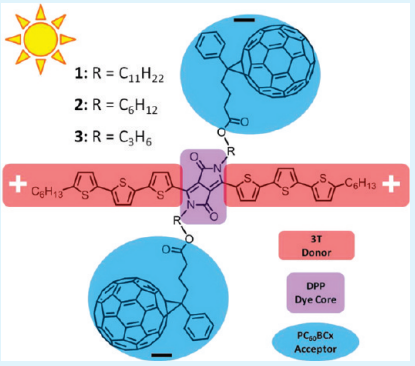

KEYWORDS: organic solar cells, diketopyrrolopyrrole, triads, *n*-type acceptor, intramolecular charge separation

INTRODUCTION

Organic solar cells (OSCs) have been investigated extensively over the last decades for their substantial future prospects in realizing low-cost solar energy conversion.[1,2] Driven by continuous research efforts in the development of new materials, processing techniques and device architectures, the power conversion efficiencies (PCEs) of OSCs have steadily improved from ∼1 % in the 1980's to ∼8% nowadays.[1−5] The most efficient OSCs to date are based on polymer/fullerene bulk heterojunctions (BHJs), wherein conjugated polymers act as electron donors, and soluble fullerenes, e.g., phenyl-$C_{61/71}$-butyric acid methyl esters ($PC_{60/70}BM$), act as electron acceptors.[6−9] One key characteristic for these high-performance systems is the nanophase separation between polymers and fullerenes, which leads to large interfaces for charge dissociation, and bicontinuous pathways for charge transport.

Recently, solution processable molecular materials with well-defined structures have attracted great attention for their many advantages over typical polymeric materials, including better monodispersity, higher purity, more reproducible and scalable synthesis, higher stability, etc.[10−15] To realize efficient solution-processed OSCs with small molecules, we require multiple functionalities for molecular semiconductors, including high solubility, strong light absorption, reasonable charge carrier mobility, and suitable self assembly property. Chemical modification of well known industrial pigments, such as quinacridone(QA) and diketopyrrolopyrrole(DPP), represents a highly promising approach to achieving low-cost molecular photovoltaic materials with desired properties. For instance, we have recently demonstrated solution processed BHJ OSCs using QA-based molecules as donors and $PC_{70}BM$ as acceptors with a PCE of 2.2 %.[10] And the most commonly investigated DPP-based molecules have yielded BHJ OSCs with efficiencies reaching as high as 4.4 %.[11] All these DPP-based electron donor molecules have linear dyad type structures, wherein the DPP core is functionalized by alkyl solubilizing groups on 2- and 5-positions and electron-rich oligothiophene units on 3- and 6-positions. The integration of electron withdrawing groups with the DPP core, on the other hand, has yielded new electron acceptors, with which PCEs of over 1% have been achieved for devices containing P3HT as the donor.[16,17] In all cases, the use of low band gap molecular materials has resulted in an significant enhancement of carrier generation in the near infrared region.[18] To further explore the functionalities of a single molecule system, we have recently prepared a series of oligothiophene-diketopyrrolopyrrole-fullerene triads (6T-DPP-$PC_{60}BC_x$, where *x* represents the number of carbon atoms on the alkyl linker, **1** [*x* = 11], **2** [*x* = 6], **3** [*x* = 3]) by covalently attaching both electron-rich and electron-accepting groups onto the DPP core (Figure 1).

Received: February 2, 2011
Accepted: June 17, 2011
Published: June 17, 2011

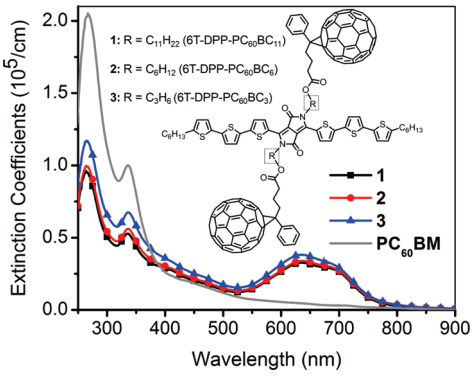

Figure 1. Absorption spectra of the neat thin films of three 6T-DPP-$PC_{60}BC_x$ triads and $PC_{60}BM$; the inset shows the molecular structures of these three compounds.

Herein, we report in-depth characterizations of these multifunctional triads in both solution and thin films, and the correlations to their device performance in OSCs and OFETs. Single component OSCs have been fabricated with PCEs approaching 0.5%, manifesting their multi-functional characteristics. Higher device performance was realized for OSCs containing P3HT as the electron donor and these molecules as the electron acceptor, exhibiting PCEs as high as 2.41%. Electron mobilities up to 1.5×10^{-3} $cm^2 V^{-1} s^{-1}$ were obtained from the OFETs of these triads. In addition, good correlations among the molecular structure, film properties and device performance have been established by combining film morphology characterizations with these device investigations.

EXPERIMENTAL SECTION

Materials. Patterned Indium tin oxide (ITO) coated glass substrates were purchased from Thin Film Devices Inc. Poly(3,4-ethylenedioxythiophene):poly(styrenesulfonate) (PEDOT:PSS) (Baytron-PH) was purchased from H. C. Starck. Poly(3-hexylthiophene) (P3HT) was purchased from Rieke Metals, Inc. Phenyl-C_{61}-butyric acid methyl ester ($PC_{60}BM$) was purchased from Nano-C Inc. All the materials were used as received without further purification. The synthesis and characterization of three triads are reported elsewhere.

Instrumentation. UV−vis absorption spectra were recorded in a Cary 5000 UV−vis−NIR spectrometer. Film thickness measurements were performed using a Dektak 150 surface profilometer. Cyclic voltammetry was performed using a 273A potentiostat from Princeton Applied Research, wherein glassy carbon acts as the working electrode, platinum as the counter electrode and a silver wire as the reference electrode. Samples were prepared in dichloromethane solution with 0.1 M tetrabutylammonium hexafluorophosphate as the electrolyte at a scan rate of 100 mV s^{-1}. The reference electrode was calibrated with an internal standard of ferrocene. Tapping-mode atomic force microscopy (AFM) was performed with a MFP-3D stand alone AFM (Asylum Research Inc.).

OSCs Fabrication and Testing. ITO glass substrates were cleaned using the following sequential steps: sonication in soap solution; rinsing with deionized water; sonication in acetone, and isopropanol for 10 min each; and drying with nitrogen. Finally, the substrates were treated with UV ozone for 10 min. A filtered dispersion of PEDOT:PSS in water was spun cast at 4000 rpm for 40 s to produce a 30 nm thick layer, followed by baking at 140 °C for 20 min in ambient. Solution processing of the active layers was performed in an inert-atmosphere (Nitrogen) glovebox. The photoactive layers containing neat triads or blends of P3HT and the triads (or $PC_{60}BM$) in different ratios were spun cast from chloroform and chlorobenzene solutions, respectively, after passing through a 0.45 μm poly(tetrafluoroethylene) (PTFE) filter. Different concentrations and spin speeds were tested in order to obtain the optimized film thicknesses. The Al cathode was evaporated through a shadow mask to produce an active area of 0.03 cm^2. After evaporation, a part of the organic layer was removed to allow contact with the ITO, and then conductive Silver paste was painted onto the exposed area in order to produce the electrical contact. All photovoltaic devices properties were measured at room temperature in a nitrogen atmosphere under AM 1.5 G solar illumination at 100 mW cm^{-2} (1 sun) using a Thermal-Oriel 300W solar simulator with filter. External quantum efficiency (EQE) values were obtained with a monochromator and calibrated with a silicon photodiode. The current density−voltage ($J-V$) characteristics were recorded in a Keithly 236 SMU.

OFETs Fabrication and Testing. Transistors were fabricated in the bottom-gate/top-contact configuration on highly doped n-type (100) Si substrates (<0.02 Ω cm) with 300-nm-thick thermally grown silicon dioxide as the dielectric layer. The Si substrates (1.4×1.6 cm^2) were successively ultrasonicated in detergent, water, acetone and isopropanol. An octadecyltrichlorosilane (OTS) monolayer was deposited by placing the substrates in 0.1 % (v/v) toluene solution overnight in the glovebox, and then ultrasonicating in toluene for 15 mins twice and dried at 130 °C. The capacitance of the gate dielectric was C_i = 15 nF cm^{-2}. The solutions were filtered through 0.45 μm PTFE filters prior to film deposition. All organic thin films were spin-coated onto the OTS layer from chlorobenzene solutions (10 mg mL^{-1}) at a rotation speed of 1000 rpm for 50 s, and the thickness of each film was measured to be around 40 nm. Finally, a 70 nm thick aluminum electrode was evaporated on top through a metal mask with channel width and length of 3 mm and 100 μm, respectively. For annealed films, thermal treatment at 120 °C for 5 min was applied before metal electrode deposition. The device characteristics were measured using Lakeshore CPX-HF probe station and Aligent 4155C Semiconductor Parameter Analyzer at room temperature under high vacuum ($\sim 1 \times 10^{-3}$ Torr).

RESULTS AND DISCUSSION

Figure 1 shows the molecular structures and the UV−vis absorption spectra of the three triads and $PC_{60}BM$ in neat thin films. Strong absorption ($\varepsilon = 1 \times 10^4$ to 1×10^5 cm^{-1}) in a broad range of 250−800 nm was observed for the triads. The low energy, broad and featureless absorption band with a peak at ~630 nm corresponds to the intramolecular charge transfer transition within the 6T-DPP conjugated unit.[14] Meanwhile the pronounced absorption in the high energy region (250−500 nm) is attributed to the attached fullerene units. The slightly higher extinction coefficient for **3** than other two compounds is due to the shorter non-photoactive alkyl linker R, affording higher molar concentration of light absorbing species within the same film thickness. The optical band gaps of ~1.60 eV for these materials were calculated from the onset of the film absorption spectra (~775 nm).

The cyclic voltammetry (CV) studies on these triads were carried out to determine the HOMO and LUMO energy levels. Multiple reversible reduction and oxidation waves were clearly observed for all three compounds (see Figure S1). The first reduction potentials of three compounds were observed at −1.12, −1.13, and −1.12 V vs. ferrocene/ferrocenium (−4.8 eV),[19] corresponding to LUMO levels of −3.68, −3.67, and −3.68 eV, respectively (Table 1). These values are close to that for $PC_{60}BM$ and much deeper than that of previously reported 6T-DPP dyad (−3.2 eV),[14] suggesting that LUMOs are mainly

localized in fullerene units and no electronic coupling between the fullerene units and the DPP core occur, which is consistent with the non-conjugating nature of the linking units. On the other hand, with the first oxidation potentials observed at 0.27, 0.25, 0.27 V vs ferrocene/ferrocenium, the HOMO levels of three compounds were calculated to be −5.07, −5.05, and −5.07, respectively. This suggests that the HOMOs are primarily delocalized on the 6T-DPP conjugated backbone as described previously for the 6T-DPP dyad.[14] As the LUMOs and HOMOs are distantly located, charge separation is expected upon light excitation, allowing for the formation of *p*/*n* junction within the triads. Correspondingly, the neat films of these triads, possessing light harvesting units as well as electron donating and accepting moieties, can be used as the single active component in OSCs.

Table 1. Physical Properties of Triads 1, 2, and 3

triad	linker	ε ($\times 10^5$ cm^{-1}) peak at ~630 nm	E_g^{opt} (eV)[a]	HOMO (eV)[b]	LUMO (eV)[b]
1	$C_{11}H_{22}$	0.33	1.60	−5.07	−3.68
2	C_6H_{12}	0.34	1.60	−5.05	−3.67
3	C_3H_6	0.38	1.60	−5.07	−3.68

[a] Estimated from the absorption edge of thin films. [b] Determined by cyclic voltammetry and calculated with reference to ferrocene (-4.8 eV vs. vacuum): $-_{HOMO} = -(-^{ox} + 4.8)$ eV, $-_{LOMO} = -(-^{red} + 4.8)$ eV.

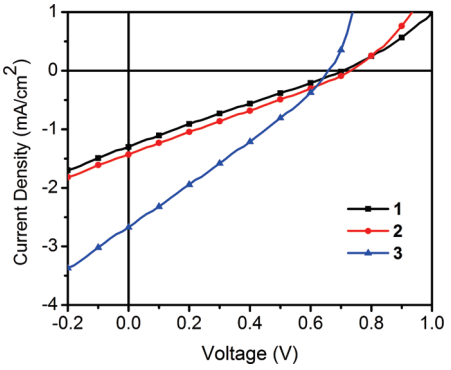

Figure 2. Current density−voltage (J−V) characteristics of organic solar cells with the device configuration of ITO/PEDOT:PSS/triad/Al under 100 mW cm^{-2}, AM 1.5 G illumination.

We have fabricated photovoltaic cells with the neat films of these multifunctional compounds, in a structure of ITO/PEDOT:PSS/Triads/Al. Figure 2 shows the current density−voltage (J−V) characteristics for the devices prepared with film thickness at ~120 nm which were thermally annealed at 150 °C for 1 min (see Figure S2 in the Supporting Information for results of as-cast devices) Table 2 summarizes important performance parameters of these devices. A PCE of ~0.5 % has been achieved for the device containing triad **3**, which is very close to the previously reported device of 6T-DPP:$PC_{60}BM$ with weight ratio of 3:7. Indeed, based on the molecular structure of triad **3**, the weight ratio of donor (6T-DPP) to acceptor ($PC_{60}BCx$) is calculated to be approximately 3:7 (see the Supporting Information), suggesting that the annealed thin film of triad **3** in neat might possess similar morphological and electronic properties as that of as-cast blends of 6T-DPP and $PC_{60}BM$. For triads **1** and **2**, the relatively long alkyl linkers account for their lower current density and device performance, as compared to triad **3**. First, due to their insulating nature, long alkyl linkers are likely to make the film less

Table 2. Device Characteristics of Organic Solar Cells (under 100 mW cm^{-2}, AM 1.5 G illumination) and Transistors with Neat Films of Triads As the Active Layer

	solar cell characteristics[a]				transistors characteristics	
active layer	V_{oc} (V)	J_{sc} (mA cm^{-2})	FF	η (%)	electron mobility (cm^2 V^{-1} s^{-1})[b]	ON/OFF ratio[c]
triad **1**	0.71	1.30	0.25	0.23	4.5 (2.8) × 10^{-4}	1000
triad **2**	0.73	1.43	0.26	0.27	6.1 (4.9) × 10^{-4}	1000
triad **3**	0.66	2.67	0.28	0.49	1.5 (1.1) × 10^{-3}	10000
6T-DPP:$PC_{60}BM$ (wt/wt = 3:7)[d]	0.63	3.13	0.27	0.53	N/A	N/A

[a] For triad-based devices, film thickness of ~120 nm, annealed at 150 °C for 1 min. [b] For triad-based devices, film thickness of ~40 nm, average mobilities for films of as-cast (values in parentheses) and annealed at 120 °C for 5 min. [c] For annealed devices. [d] OSCs results from ref 14.

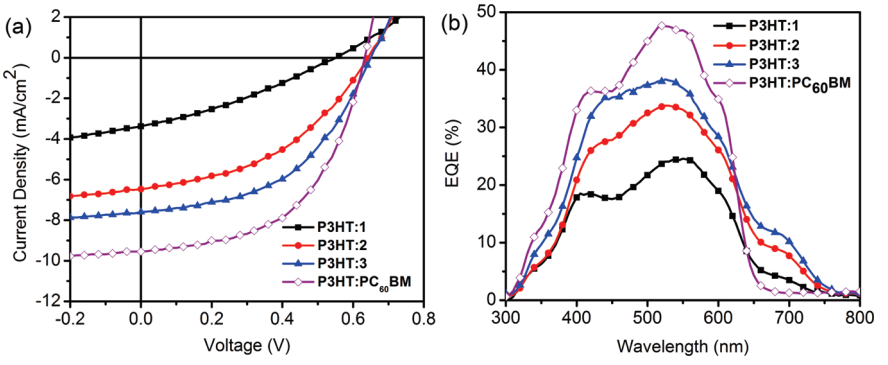

Figure 3. (a) Current density−-voltage (J−V) characteristics of devices containing the blends of P3HT and three triads as well as $PC_{60}BM$, under 100 mW cm^{-2}, AM 1.5 G illumination; and (b) EQE spectra for devices based on P3HT and three triads as well as $PC_{60}BM$.

conductive, lowering the charge transport efficiency. Second, the increase in the distance between donor and acceptor moieties might lower the charge separation efficiency, although it could result in lower recombination rate and consequently higher open circuit voltages.[20]

To evaluate the charge transport properties of these triads, thin film field effect transistors have been fabricated and tested. All materials show good n-type electron transport characteristics (triad **3** as an example in Figures S3 and S4 in the Supporting Information). Upon thermal annealing, the electron mobility is slightly improved because of more organized molecular stacking. Triad **3** exhibited much higher electron mobility than triads **1** and **2**, which testifies the above statement that longer alkyl linkers have negative effects on the charge transport properties. Nevertheless, the electron mobilities of these triads are more than one magnitude lower than that of neat film of $PC_{60}BM$ (4.1×10^{-2} cm^2 V^{-1} s^{-1})). Moreover, the hole mobilities of these films are significantly low (not detectable in our OFETs measurements), resulting in unbalanced charge carrier transport within the neat films that presumably accounts for the low performance of neat film OSC devices.

Table 3. Summary of the Best OSC Device Performance for the Blends of P3HT and Three Triads As Well as $PC_{60}BM$, under 100 mW cm^{-2}, AM 1.5 G Illumination

P3HT:acceptor (w/w) = 1.5:1	V_{oc} (V)	J_{sc} (mA cm^{-2})	FF	η (%)
triad **1**	0.55	3.38	0.31	0.58
triad **2**	0.64	6.47	0.44	1.81
triad **3**	0.65	7.60	0.49	2.41
$PC_{60}BM$	0.63	9.54	0.53	3.20

It is well-known that the device performance of photovoltaic cells is strongly dependent on the ratio of electron donor to acceptor in the active layer. In particular, for the blends of 6T-DPP and $PC_{60}BM$, high performance with a PCE of 2.33 % has been achieved with a weight ratio of donor to acceptor at 7:3, wherein a more balanced charge transport is realized. Thus, blending these triads, which have a calculated weight ratio of

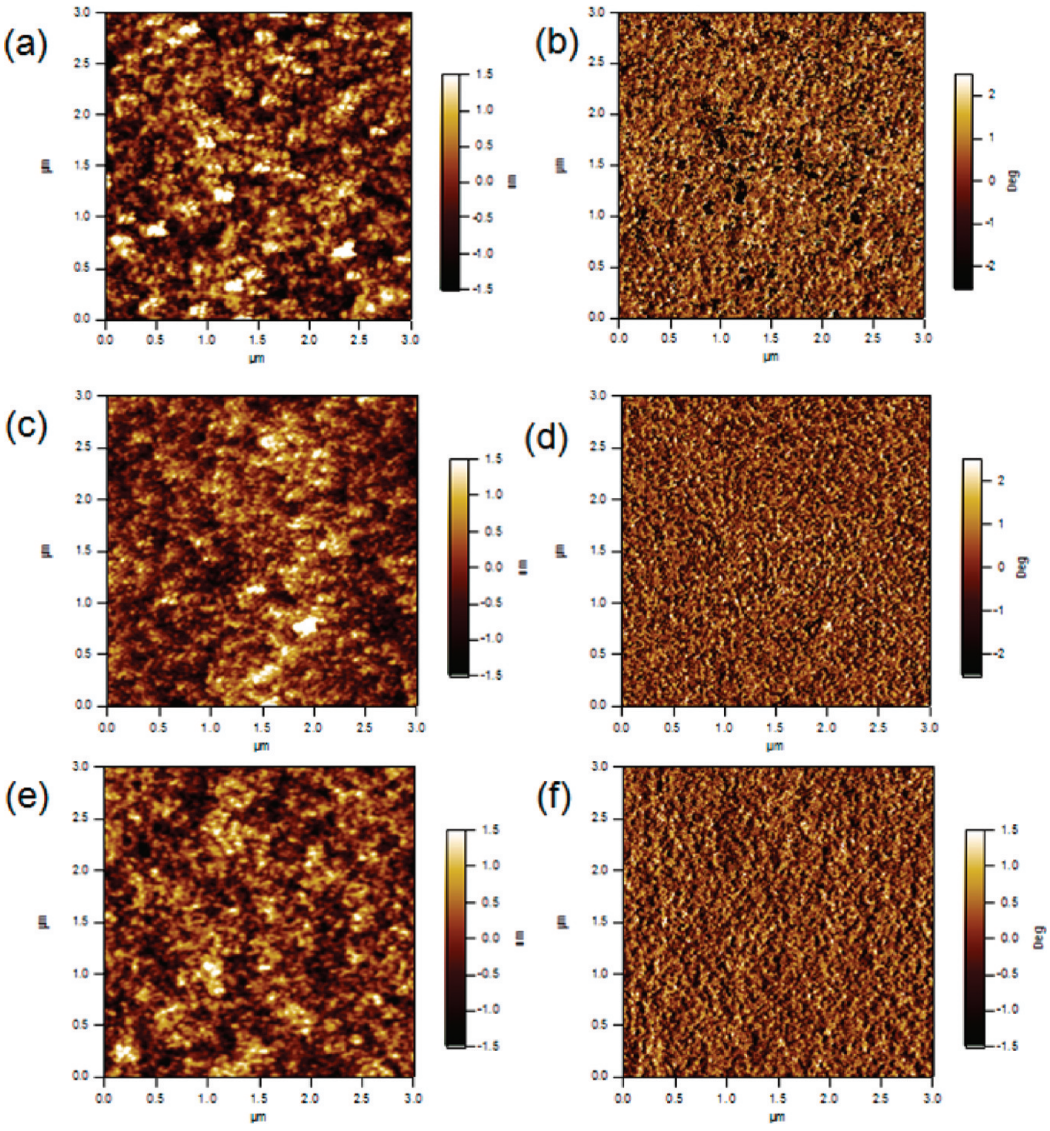

Figure 4. Tapping mode AFM topography (left) and phase (right) images of P3HT:triad devices fabricated with a ratio of 1.5:1 (a, b) P3HT:triad **1**, (c, d) P3HT:triad **2**, and (e, f) P3HT:triad **3**.

donor to acceptor at ~3:7, with a certain amount of electron donor would likely improve the device performance. This hypothesis was verified by fabricating OSC devices using blends of P3HT and these triads with a structure of ITO/PEDOT:PSS/P3HT:triad/Al. Control devices of P3HT:$PC_{60}BM$ were also fabricated for comparison. The results reported here are for devices with film thickness of ~70−80 nm, which were prepared by spin coating chlorobenzene solutions (20 mg mL^{-1}) with a weight ratio of P3HT to triads at 1.5:1. The devices were thermally annealed under various conditions for optimal performance. Annealing at 120 °C for 1 min was found to deliver the highest efficiencies for devices containing P3HT and these triads (Figures S6 and S7 in the Supporting Information show $J-V$ curves before and after annealing).

Figure 3 shows the current density−voltage ($J-V$) characteristics and external quantum efficiency spectra and Table 3 summarizes important performance parameters of these devices. (average PCEs in Table S1) It is found that the device of P3HT:triad **3** exhibited significantly higher performance than the other two P3HT:triad devices, which is consistent with the respective neat film devices. The external quantum efficiency curves exhibit a broad spectrum response covering 300−750 nm, indicating contributions to photocurrent from both P3HT and triads, with 650−750 nm particularly from the DPP core. A PCE of 2.41% has been achieved for the P3HT:triad **3** device, which is lower than that of P3HT:$PC_{60}BM$. This relatively lower performance can be mainly attributed to the lower electron mobilities and unbalanced hole and electron mobilities of these triads as shown from the space charge limited current (SCLC) data (see Table S3 in the Supporting Information). Given that the absorbance of all three P3HT:triad devices are similar (see Figure S5 in the Supporting Information), the differences in the performance among the devices can be explained by the SCLC mobility; that is, P3HT:triad **3** has the highest electron and hole mobility and best balance as compared to triad **1** and triad **2**. To evaluate the impact of film morphology on the device performance, we used tapping mode atomic force microscopy (AFM) to characterize all three films with P3HT:triads blends. Figure 4 shows the AFM images of films after thermal annealing. Overall, the films are continuous and smooth with nanoscale phase separation. And no significant difference in roughness and phase separation scale was observed for three blends of P3HT and triads (the root mean-square-average R_a at 0.63, 053, and 0.53 nm for three films respectively), suggesting electron mobility is the key to the device performance in these systems. This approach of covalently attaching low band gap sensitizer to the acceptor enables the extension of absorption without suffering from the issue of phase separation that occurs in the multicomponent system with blending of small molecule sensitizers.[18]

CONCLUSIONS

In conclusion, we have characterized a series of multifunctional small-molecule semiconductors and investigated their applications in electronic devices. According to a careful molecular design, these triads have been prepared to exhibit great solubility, strong and broad absorption and suitable energy levels. Solution-processed organic solar cells fabricated with these triads as active materials have shown high power conversion efficiencies, i.e., up to 0.5 % for neat films, and 2.4 % for the devices with blends of P3HT and these triads under an AM 1.5G simulated solar illumination. The intense and broad absorption of these triads has allowed for photocurrent generation in visible and near infrared regions. We have also shown that the molecular structure, in particular the length of alkyl linker in the triads, has significant effects on the electronic properties and subsequently device characteristics. Our work suggests a promising route to realizing high performance organic solar cells with integrated multifunctional small molecule systems. Further improvement of PCEs could be realized by the optimization of hole and electron carrier mobilities and their balance in devices.

ASSOCIATED CONTENT

Supporting Information. Additional material and device characterization data (PDF). This material is available free of charge via the Internet at http://pubs.acs.org.

AUTHOR INFORMATION

Corresponding Author
*E-mail: BWMa@lbl.gov (B.M.); atamayo@mines.edu (A.T.).

ACKNOWLEDGMENT

This work was performed at the Molecular Foundry, Lawrence Berkeley National Laboratory, and was supported by the Office of Science, Office of Basic Energy Sciences, Scientific User Facilities Division, U.S. Department of Energy, under Contract DE-AC02-05CH11231. A.T. thanks Colorado School of Mines (CSM) for financial support.

REFERENCES

(1) Tang, C. W. *Appl. Phys. Lett.* **1986**, *48*, 183–185.
(2) Yu, G.; Gao, J.; Hummelen, J. C.; Wudl, F.; Heeger, A. J. *Science* **1995**, *270*, 1789–1791.
(3) Li, G.; Shrotriya, V.; Huang, J. S.; Yao, Y.; Moriarty, T.; Emery, K.; Yang, Y. *Nat. Mater.* **2005**, *4*, 864–868.
(4) Ma, W. L.; Yang, C. Y.; Gong, X.; Lee, K.; Heeger, A. J. *Adv. Funct. Mater.* **2005**, *15*, 1617–1622.
(5) Liang, Y. Y.; Yu, L. P. *Acc. Chem. Res.* **2010**, *43*, 1227–1236.
(6) Backer, S. A.; Sivula, K.; Kavulak, D. F.; Frechet, J. M. J. *Chem. Mater.* **2007**, *19*, 2927–2929.
(7) Thompson, B. C.; Frechet, J. M. J. *Angew. Chem., Int. Ed.* **2008**, *47*, 58–77.
(8) Ross, R. B.; Cardona, C. M.; Guldi, D. M.; Sankaranarayanan, S. G.; Reese, M. O.; Kopidakis, N.; Peet, J.; Walker, B.; Bazan, G. C.; Van Keuren, E.; Holloway, B. C.; Drees, M. *Nat. Mater.* **2009**, *8*, 208–212.
(9) He, Y. J.; Chen, H. Y.; Hou, J. H.; Li, Y. F. *J. Am. Chem. Soc.* **2010**, *132*, 1377–1382.
(10) Chen, J. J. A.; Chen, T. L.; Kim, B.; Poulsen, D. A.; Mynar, J. L.; Frechet, J. M. J.; Ma, B. W. *ACS Appl. Mater. Interfaces* **2010**, *2*, 2679–2686.
(11) Walker, B.; Tomayo, A. B.; Dang, X. D.; Zalar, P.; Seo, J. H.; Garcia, A.; Tantiwiwat, M.; Nguyen, T. Q. *Adv. Funct. Mater.* **2009**, *19*, 3063–3069.
(12) Hains, A. W.; Liang, Z. Q.; Woodhouse, M. A.; Gregg, B. A. *Chem. Rev.* **2010**, *110*, 6689–6735.
(13) Ma, B. W.; Woo, C. H.; Miyamoto, Y.; Frechet, J. M. J. *Chem. Mater.* **2009**, *21*, 1413–1417.
(14) Tamayo, A. B.; Walker, B.; Nguyen, T. Q. *J. Phys. Chem. C* **2008**, *112*, 11545–11551.
(15) Mauldin, C. E.; Piliego, C.; Poulsen, D.; Unruh, D. A.; Woo, C.; Ma, B. W.; Mynar, J. L.; Frechet, J. M. J. *ACS Appl. Mater. Interfaces* **2010**, *2*, 2833–2838.

(16) Karsten, B. P.; Bijleveld, J. C.; Janssen, R. A. J. *Macromol. Rapid Commun.* **2010**, *31*, 1554–1559.
(17) Sonar, P.; Ng, G. M.; Lin, T. T.; Dodabalapur, A.; Chen, Z. K. *J. Mater. Chem.* **2010**, *20*, 3626–3636.
(18) Peet, J.; Tamayo, A. B.; Dang, X. D.; Seo, J. H.; Nguyena, T. Q. *Appl. Phys. Lett.* **2008**, 93.
(19) Pommerehne, J.; Vestweber, H.; Guss, W.; Mahrt, R. F.; Bassler, H.; Porsch, M.; Daub, J. *Adv. Mater.* **1995**, *7*, 551–554.
(20) Perez, M. D.; Borek, C.; Forrest, S. R.; Thompson, M. E. *J. Am. Chem. Soc.* **2009**, *131*, 9281–9286.